Available online at www.sciencedirect.com
ScienceDirect
Applied Catalysis B: Environmental 75 (2007) 157–166
APPLIED CATALYSIS B: ENVIRONMENTAL
www.elsevier.com/locate/apcatb

Studies of the activation process over Pd perovskite-type oxides used for catalytic oxidation of toluene

J.-M. Giraudon [a,*], A. Elhachimi [a], F. Wyrwalski [b], S. Siffert [b], A. Aboukaïs [b], J.-F. Lamonier [b], G. Leclercq [a]

[a] *Unité de Catalyse et de Chimie du Solide, UMR CNRS 8181, USTL, Bâtiment C3, 59655 Villeneuve d'Ascq, France*
[b] *Laboratoire de Catalyse et Environnement, EA 2598, Université du Littoral-Côte d'Opale, 145, Avenue Maurice Schumann, 59140 Dunkerque, France*

Received 15 July 2006; received in revised form 3 April 2007; accepted 5 April 2007
Available online 12 April 2007

Abstract

Calcined and reduced catalysts $Pd/LaBO_3$ (B = Co, Fe, Mn, Ni) were used for the total oxidation of toluene. Easiness of toluene destruction was found to follow the sequence based on the T_{50} values (temperature at which 50% of toluene is converted): $Pd/LaFeO_3 > Pd/LaMnO_{3+\delta} > Pd/LaCoO_3 > Pd/LaNiO_3$. In order to investigate the activation process (calcination and reduction) in detail, the reducibility of the samples was evaluated by H_2-TPR on the calcined catalysts. Additionally, characterization of the $Pd/LaBO_3$ (B = Co, Fe) surface was carried out by X-ray photoelectron spectroscopy (XPS) at each stage of the global process, namely after calcination, reduction and under catalytic reaction at either 150 or 200 °C for $Pd/LaFeO_3$ and either 200 or 250 °C for $LaCoO_3$. The different results showed that palladium oxidized entities were totally reduced after pre-reduction at 200 °C for 2 h (2 L/h, 1 °C/min). As $LaFeO_3$ was unaffected by such a treatment, for the other perovskites, the cations B are partially reduced as B^{3+} (B = Mn) or B^{2+} even to B^0 (B = Co, Ni). In the reactive stream (0.1% toluene in air), Pd^0 reoxidized partially, more rapidly over Co than Fe based catalysts, to give a Pd^{2+}/Pd^{4+} and $Pd^0/Pd^{2+}/Pd^{4+}$ surface redox states, respectively. Noticeably, reduced cobalt species are progressively oxidized on stream into Co^{3+} in a distorted environment. By contrast, only the lines characteristic of the initial perovskite lattice were detected by XRD studies on the used catalysts. The higher activity performance of $Pd/LaFeO_3$ for the total oxidation of toluene was attributed here to a low temperature of calcination and to a remarkable high stability of the perovskite lattice whatever the nature of the stream which allowed to keep a same palladium dispersion at the different stages of the process and to resist to the oxidizing experimental conditions. On the contrary, phase transformations for the other perovskite lattices along the process were believed to increase the palladium particle size responsible of a lower activity.

Keywords: Palladium; Perovskite; XPS; Catalytic oxidation

1. Introduction

Volatile organic compounds (VOCs) are considered to represent a serious environmental problem. Thus, the development of new active catalysts for deep oxidation of VOCs is highly desired from the viewpoint of environmental protection. The function of the catalyst is to convert the polluting compound into relatively harmless compounds at low operating temperatures and high space velocities [1]. Supported precious metals such as Pt and Pd are well established as efficient catalysts for VOCs conversion [1–3] and palladium is often more active than Pt [2]. While Pd is usually supported on Al_2O_3 for industrial applications, searching for a promoting effect is highly desirable. Indeed palladium has been incorporated into a zeolite framework to lead to interesting results for VOCs conversion [4,5]. Noteworthy, previous studies have also clearly shown the importance of the pretreatments before VOCs oxidation on such systems, thus reduction of noble metal oxides prior catalytic testing allows to speed up the reaction [6] and was attributed to a great number of Pt^0 atoms considered as active sites. It has been shown previously [7], for three-ways catalysis, that noble metals (Pd, Pt, Rh) supported on CeO_2, which is considered as a support with mobile oxygen species, greatly increases the oxidation rate of the pollutants in

* Corresponding author. Tel.: +33 3 20 43 68 56; fax: +33 3 20 43 65 61.
E-mail address: jean-marc.giraudon@univ-lille1.fr (J.M. Giraudon).

0926-3373/$ – see front matter © 2007 Elsevier B.V. All rights reserved.
doi:10.1016/j.apcatb.2007.04.005

comparison with Pd/Al_2O_3. With respect to these results the aim of our study was to find a synergetic effect by associating a noble metal, good oxidation catalyst with a lanthanum type perovskite $LaBO_3$. Indeed the noble metal at the metallic state is well known to activate the VOC by adsorption in a more efficient manner than the metallic oxides. Otherwise the perovskites, due to the great mobility of oxygen and to the redox properties associated with the transition metal B allowing to create poor ($LaCoO_{3-\delta}$) or rich oxygen ($LaMnO_{3+\delta}$) phases are considered as good catalysts for the total oxidation of VOCs.

These abilities of palladium and perovskites have motivated our present investigation to use reduced perovskite supported palladium $Pd/LaBO_3$ (B = Co, Mn, Fe, Ni) as efficient catalysts for deep oxidation of toluene (VOC which is often found in industrial exhausts). The obtaining of a noble metal beforehand reduced on the perovskite makes necessary an appropriate reduction treatment in order to try not to reduce the B transition metal cation. Consequently, if emphasis is given here on the comprehension of the global process (calcination, reduction, toluene oxidation), the effect of the reduction treatment and of phase transformations occurring on reactive stream (toluene/air) on the surface of the catalysts were particularly studied and tentatively correlated with the performances of the catalysts.

2. Experimental

2.1. Catalysts preparation

The perovskites were synthesized following preparation modes adapted from the literature [8,9]. $LaBO_3$ (B = Co, Fe, Ni) perovskites were prepared from citrate precursors. $La(NO_3)_3{\cdot}6H_2O$ (Fluka, >99%) and B nitrate salts ($Co(NO_3)_2{\cdot}6H_2O$ (Fluka, >98%); $Ni(NO_3)_2{\cdot}6H_2O$ (Prolabo, 98%); $Fe(NO_3)_2{\cdot}9H_2O$ (Fluka, 98%)) were mixed together in a suitable proportion in a minimum of water. Stoichiometric amount of citric acid (CA: Prolabo >99.7%,) ($n_{CA}/(n_B + n_{La}) = 1$) dissolved in water was then added to the resulting solution which was maintained at 100 °C for 12 h. After evaporation under reduced pressure at 70 °C a viscous gel was obtained. It was dried in an oven at 100 °C for 10 h, grounded and finally calcined at 700 °C (B = Fe) or 800 °C (B = Co, Ni) for 5 h. $LaMnO_{3+\delta}$ was prepared according to a Pechini derived method. A suitable amount of $Mn(CH_3CO_2)_2{\cdot}4H_2O$ (Prolabo, 99%) was dissolved in CA with an excess of ethylene glycol (EG: Prolabo, 99.7%) ($(n_{CA}/n_B) = 4$; $n_{EG}/n_{CA} = 1.38$). After evaporation the gel obtained was dried and grounded as above. The solid was finally calcined at 700 °C for 5 h. $Pd/LaBO_3$ were prepared by impregnating the perovskite carrier with an aqueous solution containing the appropriate amount of $Pd(NO_3)_3$ (Alfa Aesar: solution, Pd 8.5%, w/w) in order to have a palladium loading of 0.5 wt.%. The mixture was submitted to evaporation by means of a rotary evaporator at 50 °C for 2 h. After drying one night at 100 °C, the desired powders were obtained.

2.2. Catalytic activity evaluation

Conversion measurements were carried out in a flow microreactor at atmospheric pressure by programmed temperature between room temperature to 225 °C (1 °C/min). The amount of loaded catalyst was 0.1 g. Prior to each evaluation, the catalyst was calcined 4 h in flowing air (2 L/h) at 400 °C, then purged with N_2 (4 L/h) for 0.5 h. A reduction was performed under flowing H_2 from room temperature to 200 °C (1 °C/min), the isotherm being kept for 2 h (2 L/h). After cooling down, the catalyst was swept with N_2 (4 L/h) for 0.5 h. For activity determination, 1800 ppmv of toluene in air flowing at 3 L/h was admitted in the reactor. A set of valves allowed bypassing the reactor to lead the feed stream directly into the gas chromatograph sampling loop, which provides a direct measurement of the VOC concentration in the feed. The outlet gas were monitored by using on-line a Varian 3600 chromatograph, equipped with a TCD and a FID. The analysis of combustion products was performed evaluating the VOC conversion ($(CO_2 + CO)/(CO_2 + CO + 7C_7H_8)$ molar ratio).

2.3. Catalysts characterization

Phase analysis was performed by X-ray powder diffraction using a Siemens D5000 or a Huber diffractometer.

BET surface areas were measured at the liquid nitrogen temperature by nitrogen adsorption.

Elemental analysis was performed at the ''Service Central de Microanalyse'' of the CNRS (Vernaison, France). Palladium content determined by plasma emission spectroscopy on catalysts after calcination was closed to 0.5% for all the samples.

The Raman spectra were recorded on a LabRAM Infinity spectrometer (Jobin Yvon) equipped with a liquid nitrogen detector and a frequency-double Nd:YAG laser supplying the excitation line at 532 nm. The spectral resolution was about 5 cm^{-1}.

H_2-Temperature-programmed reduction experiments for the Pd-supported perovskites were carried out with an Altarima AMI-200 apparatus. The calcined samples were treated under flowing argon (30 mL/min) from room temperature to 150 °C for 1 h (5 °C/min) then cooled down to −50 °C and kept at that temperature for 15 min. The TPR were performed in a 5% H_2/Ar (50 mL/min), with a heating rate of 5 °C/min from −40 to 500 °C.

Pulse chemisorption measurements were performed using the same apparatus. The calcined samples were pre-treated for 2 h in a flow of hydrogen diluted in Ar (5%H_2/Ar; 30 mL/min) for 2 h. The sample was then exposed to a flow of argon from RT to 400 °C in order to get rid off hydrogen excess for 2 h before to be cooled down to 100 °C. Pulse chemisorption measurements were performed at that temperature with 5%H_2/Ar (30 mL/min).

XPS analysis was performed with a VG ESCALAB 220XL spectrometer. The analysis chamber was operated under ultrahigh vacuum with a pressure close to 5×10^{-7} Pa. X-rays were produced by a monochromatized aluminium anode

(1486.6 eV) radiation (15 kV, 20 mA). For these measurements, the binding energy (BE) values were referred to the C 1s photopeak at 285 eV. The surface atomic ratios were calculated by correcting the intensity with theoretical sensibility factors based on the Scofield cross section. Peak decomposition was performed using the Eclipse software from VG. The following peak intensities were used for the quantitative analysis: Pd 3d, O 1s, Co 2p, C 1s, Fe 3p. The sample was deposited in a glass support. The successive treatments performed on the catalyst were: calcination at 300 °C for 1 h in flowing air (2 L/h, 2 °C/min) followed by one night in flowing air at room temperature, reduction at 200 °C for 2 h in flowing H_2 (2 L/h, 2 °C/min) followed by one night in the catalytic chamber, treatment under reactive stream (0.1% toluene in air, 110 mL/min) from room temperature to 150 or 200 °C for $Pd/LaFeO_3$ and to 200 or 250 °C for $Pd/LaCoO_3$.

3. Results

3.1. Catalysts characterization

XRD patterns of the fresh $Pd/LaBO_3$ samples given in Fig. 1 show only the perovskite structure: a rhombohedral phase for $LaCoO_3$, $LaNiO_3$ as for $LaMnO_{3+\delta}$ and an orthorhombic one for $LaFeO_3$.

The Raman spectra of the supported catalysts are reported in Fig. 2. The Raman spectrum of $Pd/LaFeO_3$ shows a large weak line at 288 cm^{-1} and two intense lines at 435 and 610 cm^{-1}. These two intense lines have been previously observed on the Raman spectrum of $LaFeO_3$ [10]. Whereas the first one corresponds to $LaFeO_3$, the second one positioned at 625 cm^{-1}, has been previously reported as two-phonon or iron impurity. Noteworthy, the authors have shown that this line decreases as the temperature of calcination increases. The Raman spectrum of $Pd/LaCoO_3$ consists of one intensive line at 398 cm^{-1} which can be related to La_2O_3 remaining impurities. The Raman spectrum of $Pd/LaMnO_{3+\delta}$ shows a broad line at 654 cm^{-1}, a similar spectrum has been previously observed for $LaMnO_{3+\delta}$ [10], however it is different from the one of Abrasev et al. [11]. The Raman spectrum of $Pd/LaNiO_3$ shows two large lines at 446 and 398 cm^{-1}. The peak position at 398 cm^{-1} corresponds to La_2O_3 [12] while the one at 446 cm^{-1} is assigned to NiO [13]. The specific surface areas of the samples range between 5 and 18 $m^2\ g^{-1}$ (Table 1).

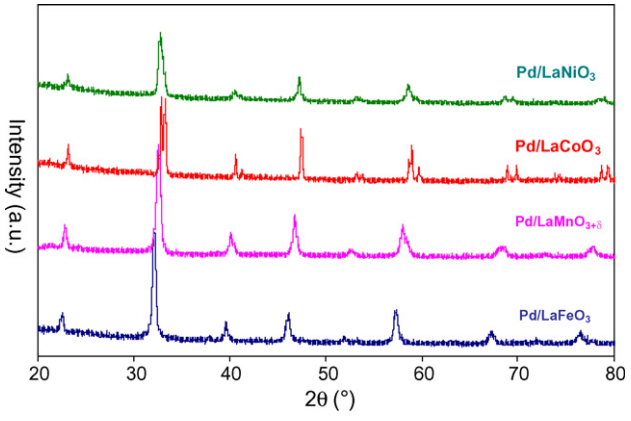

Fig. 1. XRD of the fresh $Pd/LaBO_3$ (B = Ni, Co, Mn, Fe) samples.

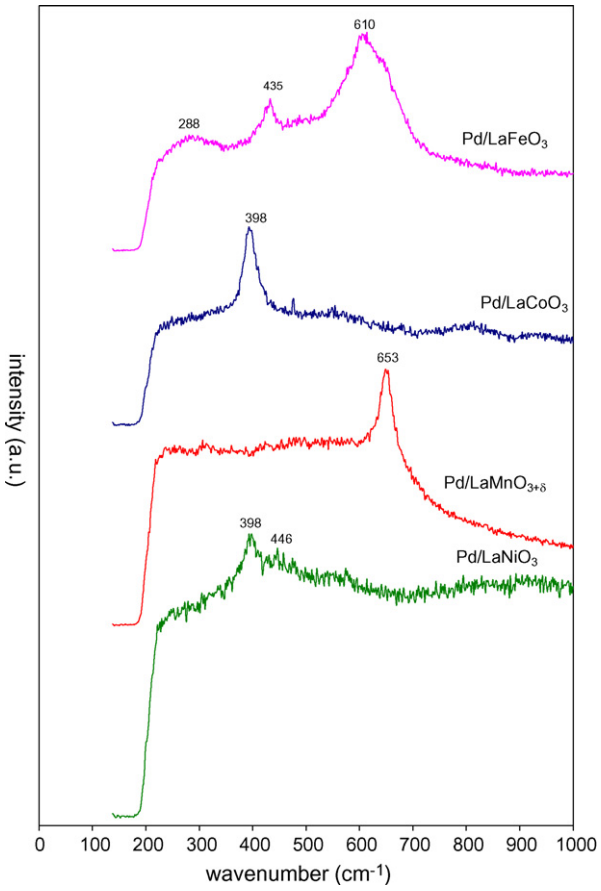

Fig. 2. Raman spectra of the fresh $Pd/LaBO_3$ samples.

3.2. H_2-TPR

Compared with the H_2-TPR curves of the perovskites [14], the reduction temperature, the reduction rate, the shape and the number of peaks are changed when adding palladium (Fig. 3 and Table 2).

The H_2-TPR trace of $Pd/LaMnO_{3+\delta}$ shows a sharp peak at 125 °C followed by a broad one at 164 °C. The first peak due to the consumption of mobile oxygen at low temperature is ascribed to the reduction of oxidized palladium entities into metallic palladium particles. The second one (H/Mn = 0.56) is due to the reduction of Mn^{4+} into Mn^{3+}.

A very weak peak at 51 °C followed by three others of decreasing intensity at 125, 219 and 296 °C are shown on the

Table 1
Specific surface areas and T_{50} of the $Pd/LaBO_3$ catalysts

	S_{BET} (m^2/g)	T_{50} (°C)
$Pd/LaFeO_3$	18	185
$Pd/LaMnO_{3+\delta}$	16	217
$Pd/LaCoO_3$	5	223
$Pd/LaNiO_3$	7	234

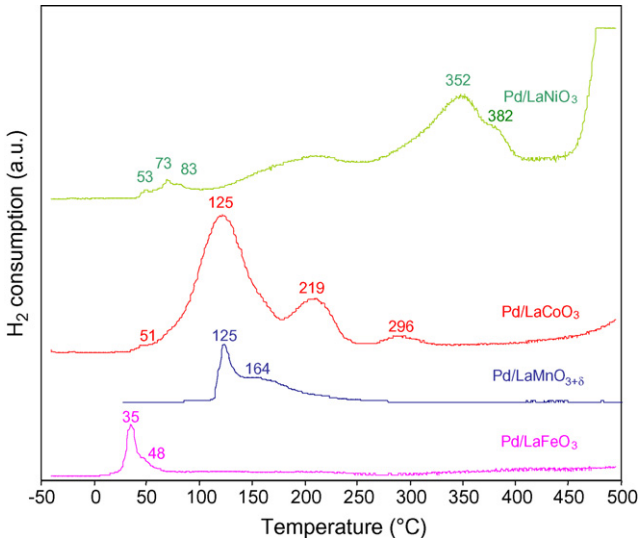

Fig. 3. H_2-TPR of the calcined Pd-supported perovskites 5% H_2/Ar (50 mL/min), 5 °C/min from −40 to 500 °C.

H_2-TPR trace of $Pd/LaCoO_3$. The first peak corresponds again to the reduction of oxidized palladium whereas the three other ones are assigned to the reduction of Co^{3+} of the perovskite into Co^{2+} then into metallic cobalt. Bustamante et al. [15] have shown that the reduction of Pd (0.15 wt%) dispersed on Co-HMOR appears at 89 °C, the temperatures of reduction of the different cobalt species being shifted to lower values compared to the zeolite alone.

On the H_2-TPR trace of $Pd/LaNiO_3$ are observed three peaks of weak intensities at, respectively, 53, 73 and 83 °C followed by a large peak at 215 °C and another at 352 °C having a shoulder at 382 °C. One notices as well the onset of a new hydrogen consumption at 430 °C. The first three peaks correspond to the reduction of different oxidized palladium and/or particles of palladium oxide differing either from their size or/and from their environments. The other following peaks are attributed to the reduction of Ni^{3+} into Ni^{2+} even into Ni metal.

The hydrogen consumption on $Pd/LaFeO_3$ shows a peak at 35 °C exhibiting a shoulder at 48 °C. The H/Pd ratio of 3.75 could be explained by the reduction of palladium species highly oxidized but also to the reduction of oxygen strongly mobile. Zhou et al. reported a temperature of reduction of oxidized palladium at 85 °C for 2.6 wt.% $Pd/LaFe_{0.8}Co_{0.2}O_3$ [16].

Hence, reducibility of palladium is influenced by the nature of the support as $Pd/LaFeO_3$ and $Pd/LaMnO_{3+\delta}$ having a rather similar specific surface area show a difference in the maxima of the first H_2 consumption of about 90 °C. The oxidized palladium reduction is easier for $Pd/LaFeO_3$ whereas it is the most difficult on $LaMnO_{3+\delta}$. The two other samples have an intermediate behaviour. Additionally, the reducibility of the perovskite is greatly enhanced when adding palladium excepted for the $Pd/LaFeO_3$ sample. Here catalytic reduction is able to account for the decrease of the temperature of reduction of the B cation when palladium is present.

Table 2
H_2-TPR results of the calcined $Pd/LaBO_3$ perovskites

	Step 1 T_{max}/°C (H/Pd)/mol/mol	Step 2 T_{max}/°C (H/B)/mol/mol
$Pd/LaCoO_3$	51 (n.d.)	125 (0.75); 219–296 (0.17)
$Pd/LaMnO_{3+\delta}$	125 (n.d.)	164 (0.56)
$Pd/LaFeO_3$	35–45 (3.75)	
$Pd/LaNiO_3$	53–73–83 (3.30)	215–352–382 (0.96)

Examination of the different H_2-TPR traces clearly shows the difficulty to selectively reduce the palladium oxide without modifying the perovskite network, $Pd/LaFeO_3$ excepted. Indeed palladium addition, in speeding up the reduction of the cation B, makes difficult the choice of a temperature of reduction which does not affect the perovskite.

3.3. H_2 chemisorption

H_2 chemisorption has been carried out by a pulse method on the two samples that have been studied by XPS and $Pd/LaMnO_{3+\delta}$. The results show that palladium is better dispersed over $LaFeO_3$ ($D = 19 \pm 2\%$) than $LaCoO_3$ ($D = 14 \pm 2\%$) and $LaMnO_{3+\delta}$ ($D = 7 \pm 2\%$). From these metal dispersion data we have determined the average metallic palladium particle diameter which is 6, 8 and 15 nm for $Pd/LaFeO_3$, $Pd/LaCoO_3$ and $Pd/Pd/LaMnO_{3+\delta}$, respectively.

3.4. XPS studies

The surface state of the $Pd/LaCoO_3$ and $Pd/LaFeO_3$ samples has been investigated by XPS at the end of the successive steps of the global process of total oxidation of toluene, that are the calcination (air, 300 °C, 6 L/h, 4 h), the reduction (H_2, 200 °C, 2 L/h, 2 h) and the exposure to the reactional atmosphere (1000 ppmv toluene in air, $F = 6$ L/h) at two temperatures which have been chosen considering the light-off curves in order to have information on the solids after catalysis performed, respectively, at a low and high conversion of

Table 3
XPS phase composition of the $Pd/LaBO_3$ catalysts

Experimental conditions	XPS composition	
	$Pd/LaCoO_3$	$Pd/LaFeO_3$
Calcination	$LaCo_{0.46}O_{2.88}Pd_{0.09}C_{0.35}$	$LaFe_{0.82}O_{2.82}Pd_{0.05}C_{0.21}$
Reduction	$LaCo_{0.64}O_{2.37}Pd_{0.08}C_{0.34}$	$LaFe_{0.79}O_{2.83}Pd_{0.05}C_{0.48}$
On stream to 200 °C (150 °C*)	$LaCo_{0.76}O_{3.81}Pd_{0.11}C_{1.9}$	$LaFe_{0.81}O_{2.99}Pd_{0.05}C_{0.88}$*
On stream to 250 °C (200 °C*)	$LaCo_{0.66}O_{4.66}Pd_{0.09}C_{1.88}$	$LaFe_{0.81}O_{3.19}Pd_{0.05}C_{1.33}$*

Table 4
Carbon to lanthanum XPS atomic ratios for $Pd/LaCoO_3$ after each step of the process

	CC/La	CO/La	CO_2/La	CO_3/La	$\pi\pi^*$/La	C_T/La
Calcination	0.175	0.0298	0.107	0.0385	–	0.35
Reduction	0.130	0.030	0.11	0.06	–	0.33
On stream[a]	1.162	0.0930	0.267	0.34	0.040	1.90
On stream[b]	1.062	0.128	0.372	0.255	0.064	1.88

[a] RT to 200 °C.
[b] RT to 250 °C.

toluene. The different results are displayed Tables 3 and 4 and Figs. 4–10.

3.4.1. *Pd/LaCoO₃*

One observes on spectrum (a) of Fig. 4 recorded after calcination the components Pd $3d_{5/2}$ and Pd $3d_{3/2}$, respectively, at 337.4 (FWHM = 1.8 eV) and 342.5 eV. The Pd $3d_{5/2}$ binding energy (BE) differs markedly from the value of 336.1–336.9 characteristic of PdO [17] and is close to the value of 337.7 eV characteristic of PdO_2 [17]. Uenishi et al. [18] reported such a rather similar value that they attributed to a cationic Pd, namely Pd^{3+} or/and Pd^{4+}, incorporated into the B-site of the perovskite under oxidation atmosphere. So different oxidized palladium entities here could account for such a high binding energy value.

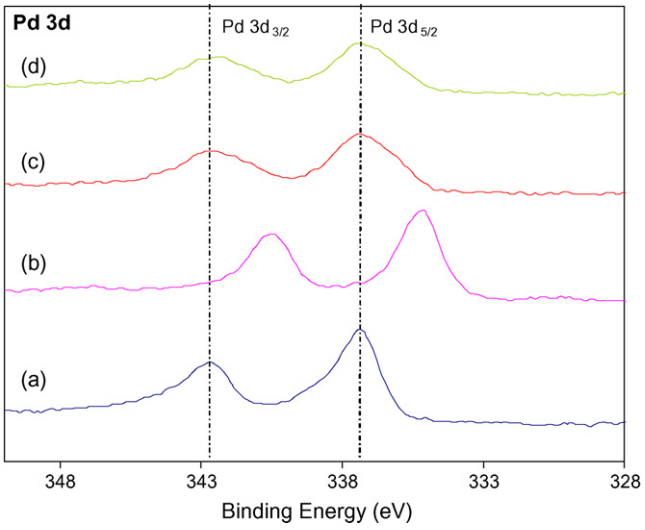

Fig. 4. Evolution of Pd 3d XPS spectrum of $Pd/LaCoO_3$ during the overall process. After: (a) calcination, (b) reduction, (c) exposure on stream from RT to 200 °C and (d) exposure on stream from RT to 250 °C.

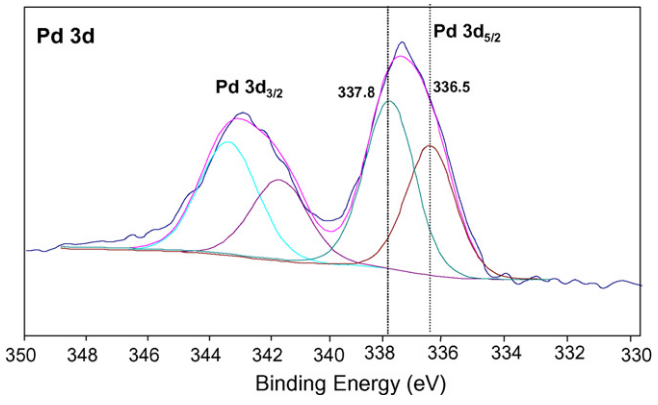

Fig. 5. Decomposition of the Pd 3d XPS spectrum of $Pd/LaCoO_3$ after exposure on stream from RT to 200 °C.

After reduction at 200 °C in pure hydrogen (spectrum (b)), the Pd $3d_{5/2}$ photopeak shifts to a lower value of 335.2 eV which corresponds to a metallic palladium [17]. Whatever the final temperature of catalyst exposure to toluene/air (spectra (c) and (d)) the Pd $3d_{5/2}$ photopeak shifts to the initial value of 337.4 eV but with a substantial FWMH increase (FWMH = 2.5 eV) indicating at least two different Pd species. Indeed, decomposition of the Pd $3d_{5/2}$ envelop (Fig. 5) shows two components at 337.8 (±0.4 eV) and 336.5 eV (±0.4 eV) values. The first one characterizes the previous Pd^{4+} phase obtained after calcination whereas the other characterizes a Pd^{2+} in accordance with PdO [17], relative atomic Pd^{4+}/Pd^{2+} proportion being of 60/40.

XPS spectrum (a) of Co 2p displayed in Fig. 6 shows dissymmetric Co $2p_{1/2}$ and Co $2p_{3/2}$ photoelectron peaks at 795.0 and 780.0 eV respectively. The difference in BE between these two components of 15 eV is consistent with the presence of Co^{3+} accordingly to the works of Okamoto et al. [19]. Besides a large signal of weak intensity at about 10 eV upscale from the Co $2p_{3/2}$ peak is detected. This satellite is characteristic of Co^{3+} in a low-spin configuration [20].

After reduction at 200 °C one sees a broadening of the Co $2p_{3/2}$ peak centred at 779.5 eV as well as an increase of the Co

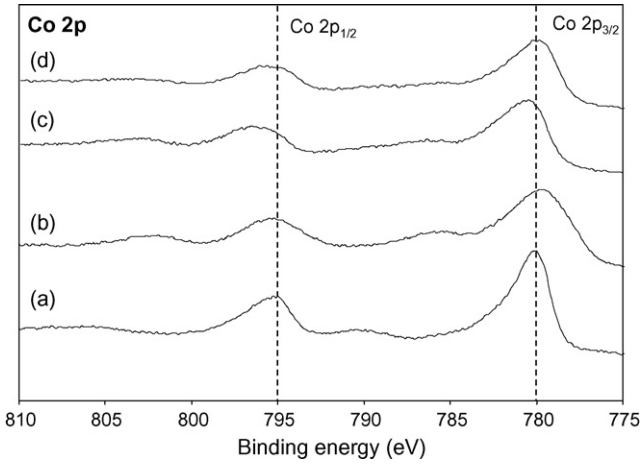

Fig. 6. Evolution of Co 2p of $Pd/LaCoO_3$ during the overall process. After: (a) calcination, (b) reduction, (c) exposure on stream from RT to 200 °C and (d) exposure on stream from RT to 250 °C.

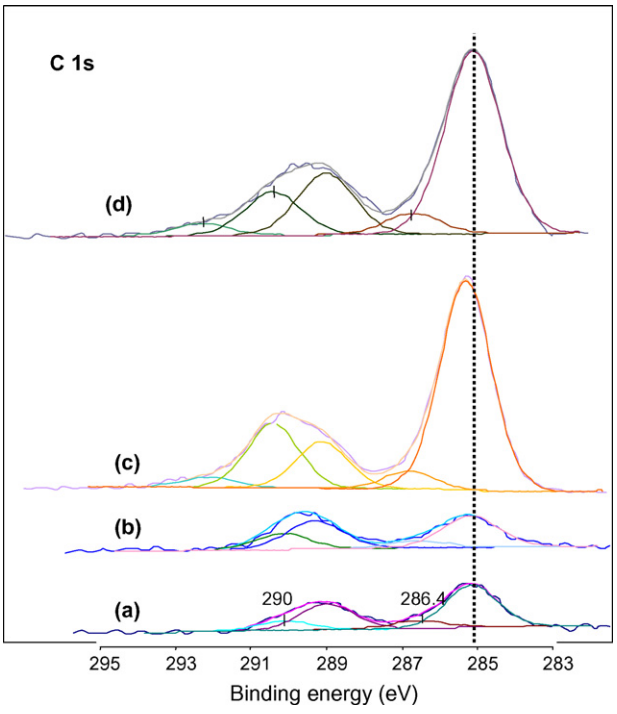

Fig. 7. Evolution of C 1s XPS spectrum of $Pd/LaCoO_3$ during the overall process. After: (a) calcination, (b) reduction, (c) exposure on stream from RT to 200 °C and (d) exposure on stream from RT to 250 °C.

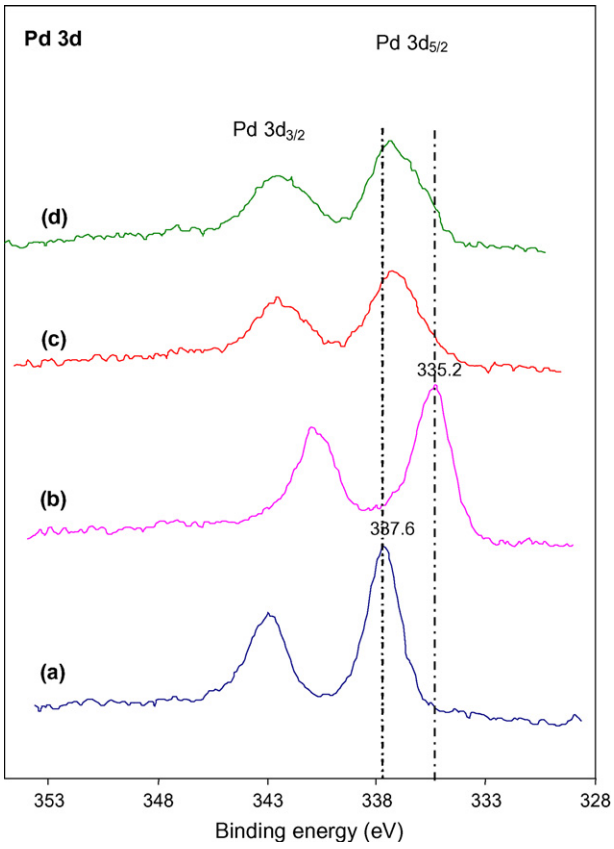

Fig. 8. Evolution of Pd 3d XPS spectrum of $Pd/LaFeO_3$ during the overall process. After: (a) calcination, (b) reduction, (c) exposure on stream from RT to 150 °C and (d) exposure on stream from RT to 200 °C.

$2p_{3/2}$–Co $2p_{1/2}$ peak separation amounting to 15.6 eV. Also an intense shake-up satellite line distant from 5.4 eV upscale from the Co $2p_{3/2}$ BE maximum is present. All these observations suggest the presence of Co^{2+} species in a distorted environment at the catalyst surface. Decomposition of the Co $2p_{3/2}$ envelop shows besides the Co $2p_{3/2}$ components at 780 eV a small component at 778.3 eV associated to Co^0 [21] whose proportion amounts to approximately 13% of the total detected cobalt.

Upon toluene/air exposure the disappearance of the Co $2p_{3/2}$ component at 778.3 eV evidences the reoxidation of metallic cobalt. Whereas the Co $2p_{3/2}$ peak position as the Co $2p_{1/2}$–Co $2p_{3/2}$ peak separation keep constant within the margin of error compared to the previous spectrum the satellite intensity, as for it, markedly decreases. Such results are consistent with a reoxidation of the reduced cobalt species into Co^{3+} in a distorted environment.

The La 3d signals after calcination and reduction are similar and show two doublets of photoelectron peaks whose components at the lowest binding energies, respectively, at 833.8 and 850.1 eV are characteristic of La $3d_{5/2}$ and La $3d_{3/2}$ associated with a La^{3+} ion in the perovskite [22]. The peaks which appear on the high energy side of the La $3d_{5/2}$ and La $3d_{3/2}$ main peaks are satellites which have been ascribed to the transfer of an oxygen-centred electron to the empty 4f shell accompanying the ionisation process [23]. After toluene/air exposure the peaks broaden and the La $3d_{5/2}$ component shifts 0.4 eV upscale. This could suggest a carbonation of excess La_2O_3 at the surface (see below) of the catalyst.

All O 1s spectra show two majors components, one at 529.2 eV characteristic of the oxygen network of the perovskite O^{2-} [24] and the other very broad peak at 531.6 ± 0.5 eV corresponding to adsorbed oxygen, OH^- and CO_3^{2-} groups [25]. After reduction a fraction of adsorbed oxygen species at high BE is removed. Upon toluene/air exposure the adsorbed oxygen phase increases at the expense of the O^{2-} one (Table 6).

Fig. 7 shows the evolution of the C1s spectra and Table 4 sums up the different XPS atomic ratios C/La. Decomposition of the C 1s envelop of spectrum (a) exhibits four components, two major ones at 285 and 288.7 eV and two minor ones at 286.4 and 290.0 eV referenced as C–C and as CO_2, the two other ones associated with carbon in interaction with oxygen are, respectively, C–O and CO_3^{2-} [26]. The different data show that after calcination (oxy)carbonaceous residues remain at the surface of the catalyst resulting from the incomplete decomposition of the citrate precursor. The spectrum (b) is rather similar to the previous one showing that the hydrogen treatment has no significant effect on carbon impurities removal. Upon reactional atmosphere (spectra (c) and (d)) a strong increase of the total carbon to lanthanum ratio Ct/La occurs, the raising of the C–C component being substantially higher than the other ones. The CO_x ($x = 1$–3) components are here mainly representative of adsorbed oxygenated organic species being partially oxidized. Noticeable is the appearance of a plasmon or shake-up satellite peak at 291.9 eV whose position is consistent with a $\pi\pi^*$ transfer arising from adsorbed benzene like species [27].

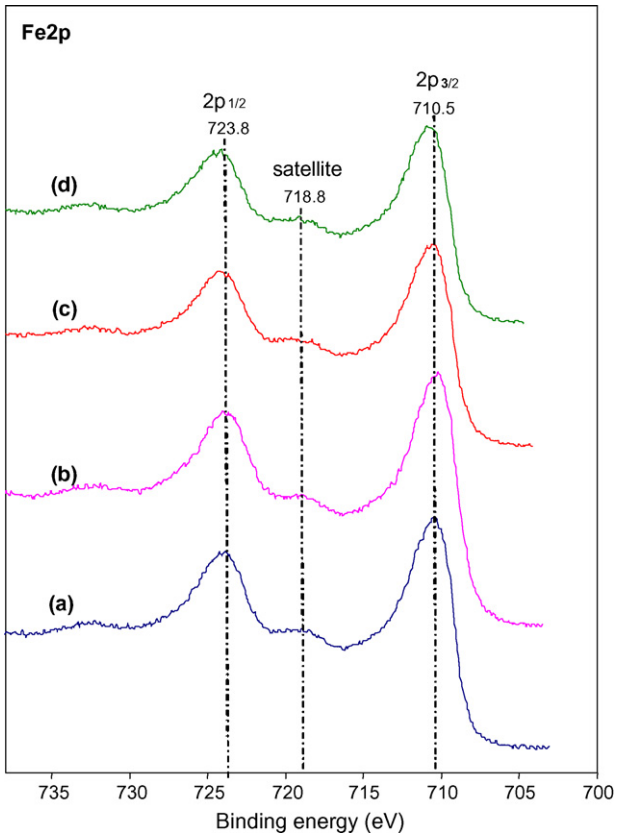

Fig. 9. Evolution of Fe 2p XPS spectrum of $Pd/LaFeO_3$ during the overall process. After: (a) calcination, (b) reduction, (c) exposure on stream from RT to 150 °C and (d) exposure on stream from RT to 200 °C.

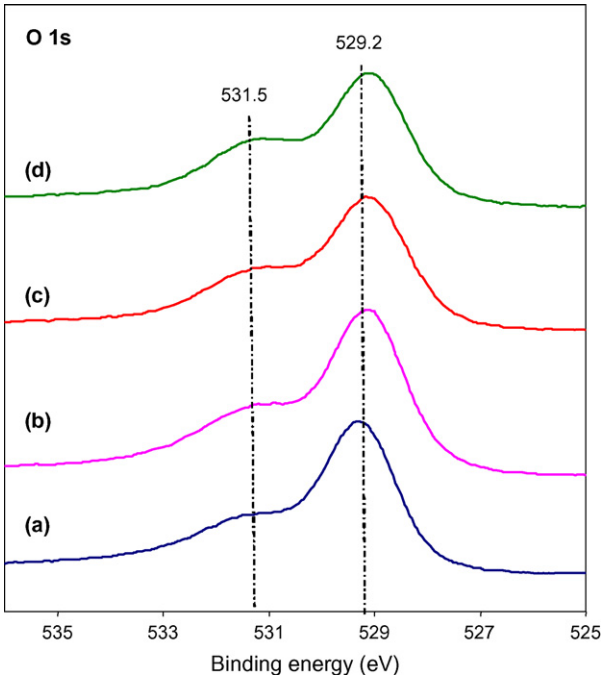

Fig. 10. Evolution of O 1s XPS spectrum of $Pd/LaFeO_3$ during the overall process. After: (a) calcination, (b) reduction, (c) exposure on stream from RT to 150 °C and (d) exposure on stream from RT to 200 °C.

The nominal XPS formula of the catalysts are given Table 3. After calcination the Co/La atomic ratio of 0.46 shows an important lanthanum excess at the surface which is substantially higher than the Co/La ratio of 0.8 found for $LaCoO_3$ in accordance with previous results reported both by Sinquin et al. [23] and Tabata et al. [28] who found a similar value starting either from propionic acid or acetate precursors on the cobalt based perovskite. XPS atomic ratio Pd/La of 0.09 which is about eight times higher than the global one shows a significant enrichment in palladium at the surface. Noteworthy is the increase of the Co/La after reduction which could be due to the diffusion of La^{3+} from the surface to the bulk or preferably due to the rising of Co^0 or Co^{2+} which have been expelled from the perovskite network to diffuse to the surface. This Pd/La ratio keeps approximately constant, with the margin of error, during the catalytic testing whatever the final temperature.

3.4.2. *Pd/LaFeO₃*

After calcination of $Pd/LaFeO_3$, the BE of Pd $3d_{5/2}$ (FWMH = 1.8 eV) at 337.6 eV suggests again a palladium oxidation in an unusual state as stated above (Fig. 8). Then Pd is found in the metallic state (Pd $3d_{5/2}$ BE = 335.2 eV) after reduction. Upon catalytic reaction in the VOC/air atmosphere (spectra (c) and (d)), the Pd $3d_{5/2}$ signal shifts of 2 eV upscale from the previous value and broadens. Decomposition of the Pd $3d_{5/2}$ envelop gives now three components at 337.5 and 336.4 and 335.2 eV, respectively, attributed to Pd^{4+}, Pd^{2+} and Pd^0 with relative abundances amounting to 60, 30 and 10%.

The different Fe 2p profiles are exhibited in Fig. 9. After calcination (spectrum (a)) the Fe $2p_{3/2}$ photoelectron peak appears asymmetric and has a BE at 710.5 eV with a distinct large and low intensity satellite peaking at about 718.8 eV attesting of a Fe^{3+} [17,29]. Spectra (b–d) which practically superimpose with spectrum (a) evidence the good stability of the perovskite network originating from the non-reducibility of the Fe^{3+} in site B.

The C 1s envelop shows upon decomposition the same components as above whose amounts relative to lanthanum are given in Table 5. A substantial increase of all the C–C and C–O_x (x = 1–3) components after VOC/air exposure is again noticed. On the other hand, the XPS atomic ratio of total carbon to lanthanum Ct/La at 200 °C of 1.33 is significantly lower than the one of 1.90 for $Pd/LaCoO_3$ at that same temperature.

The La 3d envelop for all spectra is composed of two well resolved doublets of photoelectron peaks whose La $3d_{5/2}$ low

Table 5
Carbon to lanthanum XPS atomic ratios for $Pd/LaFeO_3$ after each step of the process

	CC/La	CO/La	CO_2/La	CO_3/La	$\pi\pi^*$/La	C_T/La
Calcination	0.0821	0.008	0.071	0.0474	–	0.21
Reduction	0.272	0.063	0.131	0.014	–	0.48
On stream[a]	0.591	0.079	0.141	0.045	0.022	0.88
On stream[b]	0.869	0.087	0.251	0.073	0.048	1.33

[a] RT to 150 °C.
[b] RT to 200 °C.

Table 6
O1s/La 2p XPS ratio for Pd/$LaBO_3$ (B = Co, Fe) after each step of the process

	Pd/$LaCoO_3$			Pd/$LaFeO_3$		
	O(I)/La	O(II)/La	O/La	O(I)/La	O(II)/La	O/La
Calcination	1.63 (531.7)	1.25 (529.1)	2.88	1.54 (530.8)	1.28 (529.2)	2.82
Reduction	1.27 (531.2)	1.10 (528.9)	2.37	1.68 (530.6)	1.15 (529.0)	2.83
On stream[a]	2.52 (532.0)	1.29 (529.1)	3.81	1.26 (5.31.8)	1.73 (529.6)	2.99
On stream[b]	3.05 (531.2)	1.61 (528.7)	4.66	1.27 (531.5)	1.91 (529.3)	3.19

[a] RT to 150 °C (B = Fe), 200 °C (B = Co).
[b] RT to 200 °C,(B = Fe), 250 °C (B = Co).

binding energy component at 833.9 eV is again characteristic of La^{3+} ion. However, it must be mentioned that the valley between each component of any doublet is better resolved than the one observed on Pd/$LaCoO_3$ which could suggest that carbonation of segregated lanthanum type oxide particles is less pronounced.

The O 1s spectra (Fig. 10) can be decomposed into two majors components already observed previously at about 529.2 ± 0.5 and 531.5 ± 0.5 eV. In contrast with Pd/$LaCoO_3$, under reactional atmosphere, the O^{2-} component is always higher than the adsorbed oxygen-containing one showing a small contribution of the O^- and oxygen adsorbed species contrarily to the Pd/$LaCoO_3$ sample (Table 6). Noteworthy, the XPS atomic ratio Fe/La of 0.82 (Table 3) obtained after calcination shows a lanthanum enrichment significantly weaker than the one relative to Pd/$LaCoO_3$ sample. The XPS atomic ratio Pd/La of 0.05 is about five time higher to the global one showing again an enrichment of palladium at the surface of the catalyst but less pronounced than previously. Moreover, the Fe/La as the Pd/La ratios keep unchanged during the overall process showing clearly the good stability of the catalyst under the different gaseous atmospheres.

3.5. Catalytic activity

The light-off curves of the four catalysts are given in Fig. 11 and the characteristic temperatures reported in Table 2. Toluene conversion starts around 130 °C for $LaCoO_3$ and $LaMnO_{3+\delta}$ and 140 °C for $LaFeO_3$ and around 200 °C for $LaNiO_3$. The conversion straightens up faster on $LaFeO_3$ as total destruction

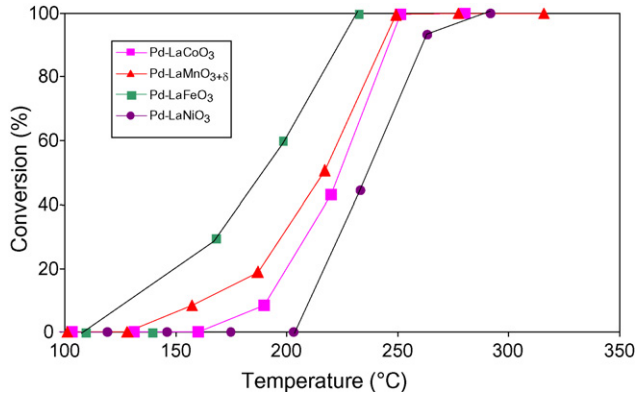

Fig. 11. Conversion of 1800 ppmv toluene in air over Pd/$LaBO_3$ (B = Co, Mn, Fe) vs. temperature (m_{cat} = 0.1 g; F_{air} = 3 L/h).

of the VOC is at 230 °C for the iron-based catalyst compared to 250 °C for the two Mn and Co related ones.

The activity of the Pd/$LaBO_3$ (based on the values of T_{50}) decreased in the order: Pd/$LaFeO_3$ > Pd/$LaMnO_{3+\delta}$ > Pd/$LaCoO_3$ > Pd/$LaNiO_3$. All the catalysts were selective in CO_2 and H_2O formation. Only traces of benzene were observed with Pd loaded on $LaMnO_{3+\delta}$.

3.6. Characterization after catalytic test

XRD has been performed on the tested catalysts. The XRD patterns for all the used catalysts only show the lines of the initial perovskites. The S_{BET} values also keep unchanged.

4. Discussion

Usually, the catalytic properties of Pd supported catalyst have been found to be dependant on the palladium dispersion and/or of the oxidation state of the noble metal which is closely related to the metal–support interaction.

Regarding the first point, it has been shown from H_2 chemisorption data, that the Pd dispersion over perovskite is poor and decreases as follow: Pd/$LaFeO_3$ (D = 19%) > Pd/$LaCoO_3$ (14%) > Pd/$LaMnO_{3+\delta}$ (7%). The dispersion does not correlate with the specific surface area of the supports neither with the activity. The $(Pd/La)_{XPS}$ ratios of 0.05 (±0.01) and 0.09 (±0.02) for Pd/$LaFeO_3$ and Pd/$LaCoO_3$, respectively, substantially higher than the nominal ratio of around 0.011 shows an enrichment of palladium. Owing to the mean free path $\lambda_{Pd^0 \rightarrow Pd^0}$ which is of 2.2 nm and to the average particle size of metallic palladium determined from the chemisorption data, the overall Pd^0 particle is expected to be probed by XPS here only for Pd/$LaFeO_3$. Hence, the $(Pd/La)_{XPS}$ atomic ratio higher for Pd/$LaCoO_3$ compared to the one of Pd/$LaFeO_3$ is difficult to be interpreted and could be due to a large particle size distribution of palladium on the samples.

Regarding now the oxidation degree of palladium, XPS results have clearly shown that after calcination, Pd oxidation state is likely +4; the value of H/Pd ratio of 3.75 close to 4 obtained by H_2-TPR for Pd/$LaFeO_3$ supports such a hypotheses. This strongly suggests the presence of cationic Pd entities to be located at the topmost atomic layer of the perovskite lattice. The reducibility of this oxidized Pd is dependent on the nature of the support, the easiness of cationic Pd reduction decreasing according to the sequence: Pd/$LaFeO_3$ > Pd/$LaCoO_3$ ≈ Pd/$LaNiO_3$ > Pd/$LaMnO_{3+\delta}$. Additionally, the reducibility of the

perovskite is greatly enhanced when adding palladium to different extents [14]. Thus, the ease of the reducibility of cation B (B^{4+} to B^{3+} for Mn; B^{3+} to B^{2+}: Co, Ni, Fe) decreases according to: $LaMnO_{3+\delta} > LaCoO_3 \approx LaNiO_3 \gg LaFeO_3$.

In pure H_2, at 200 °C for 2 h, Pd^{4+} is totally reduced into Pd^0 for each catalyst in accordance with H_2-TPR results. Regarding the reduction of the perovskite network, XPS studies show that Co^{3+} is reduced into Co^{2+} with a distorted environment and into Co^0, whereas $LaFeO_3$ network is preserved. Based on TPR results the oxygen overstoichiometry of the perovskite lattice is expected to be lost for $Pd/LaMnO_{3+\delta}$ leading to $Pd/LaMnO_3$. Under flowing reactive stream, as metallic palladium totally reoxidizes to give Pd^{+4} and Pd^{+2} on $Pd/LaCoO_3$, a small fraction of palladium keeps at the metallic state whatever the ending temperature of the catalytic test for $Pd/LaFeO_3$. Enhancement of resistance of metallic palladium particle towards oxidation for $Pd/LaFeO_3$ compared to $Pd/LaCoO_3$ could be explained by a better electronic transfer from the Pd particles to the acidic Lewis sites of the perovskite. Detection of both Pd^{4+} and Pd^{2+} can be tentatively explained by a migration of one fraction of metallic palladium into the sites B of the topmost layers of the perovskite while the remaining part stays at the surface of the catalyst as PdO particles. As $LaFeO_3$ is preserved during the test, reconstruction of the perovskite lattice takes place in the bulk of the material on reactive stream for the others samples to give $LaCoO_3$, $LaNiO_3$ and $LaMnO_{3+\delta}$ as seen by XRD on the used catalysts. On the other hand the cobalt cation site is still altered at the surface of the catalyst at the final temperature.

Considering the catalytic performances of the $Pd/LaBO_3$ samples we show that there is a clear relation between the activity and the perovskite lattice stability which is related to the reductibility of the B cation. As metallic palladium speeds up significantly the Co, Ni and Mn cation reduction, stabilization of Pd in a metallic state is accompanied with a reduction of the perovskite. In $Pd/LaCoO_3$ and $Pd/LaNiO_3$, Co^{3+} (Ni^{3+}) likely transforms into Co^{2+} (Ni^{2+}) and metallic Co (Ni) after reduction leading to a partial degradation of the perovskite network. In $Pd/LaMnO_{3+\delta}$, transformation of $LaMnO_{3+\delta}$ into $LaMnO_3$ occurs in our experimental conditions based on H_2-TPR results. Here the extent of the perovskite network destruction is believed to decrease owing to $Pd/LaCoO_3 \approx Pd/LaNiO_3 > Pd/LaMnO_{3+\delta}$. These types of transformation have been responsible owing to Mitachi and co-workers [30] to an increase of the Pd particle size because the perovskite grains grew. One other possible consequence could be a change in the ability of palladium to adsorb oxygen [31].

The order of decreasing resistivity against oxidation corresponds to $Pd/LaFeO_3 > Pd/LaCoO_3$. Here the smaller Pd° particles of $Pd/LaFeO_3$ seem to be oxidized at a slower rate compared to the larger ones of $Pd/LaCoO_3$ showing probably the importance of the acido-basic properties of the support in the global electronic transfer between Pd and the perovskite. By comparaison, Yazawa et al. have clearly shown that palladium on acidic support kept the metallic state under high oxygen concentration, indicating that acidic support gives palladium the resistivity against oxidation [32]. Such a support effect has been observed by Ishikawa et al. in propane combustion over platinum catalysts [33].

The high activity of $Pd/LaFeO_3$ can be attributed here to the a better Pd dispersion due the high surface area of $LaFeO_3$ which has been calcined at the lowest temperature, and also to the remarkably high stability of $LaFeO_3$ structure in the overall process which keeps Pd in a same dispersion state whatever its oxidation degree. By contrast, for the others samples, perovskite transformations occurring during the overall process due partial reduction of the perovkite network after H_2 pre-reduction can adversely increase the palladium size and decrease the catalyst conversion.

5. Conclusion

Calcined and reduced $Pd/LaBO_3$ (B = Co, Fe, Mn, Ni) were used as catalysts for the total oxidation of toluene. Among these catalysts $Pd/LaFeO_3$ sample shows the best catalytic properties. The higher activity performance of $Pd/LaFeO_3$ for the total oxidation of toluene was attributed here to a low temperature of calcination and to a remarkable high stability of the perovskite lattice whatever the nature of the stream which allowed to keep a same palladium dispersion at the different stages of the process and to resist to the oxidizing experimental conditions. On the contrary, phase transformations for the other perovskite lattices along the process were believed to increase the palladium particle size responsible of a lower activity.

Acknowledgement

We thank the European community through an interreg 3 France-Wallonie-Flandre project for financial supports.

References

[1] J.J. Spivey, Ind. Eng. Res. 26 (1987) 2165.
[2] G. Centi, J. Mol. Catal. 173 (2001) 287.
[3] K. Okumura, T. Kobayashi, H. Tanaka, M. Niwa, Appl. Catal. B: Environ. 44 (2003) 325.
[4] M. Guisnet, P. Dégé, P. Magnoux, Appl. Catal. B: Environ. 20 (1999) 1.
[5] P. Dégé, L. Pinard, P. Magnoux, Appl. Catal. B: Environ. 27 (2000) 17.
[6] P. Dégé, L. Pinard, P. Magnoux, M. Guisnet, C.R. Acad. Sci. 4 (2001) 41.
[7] P. Granger, L. Delannoy, J.J. Lecomte, C. Dathy, H. Praliaud, L. Leclercq, G. Leclercq, J. Catal. 207 (2002) 202.
[8] S. Irusta, M.P. Pina, M. Menedez, J. Santamaria, J. Catal. 179 (1998) 400.
[9] M.P. Pechini, US Patent, 330,697 (1967).
[10] M. Popa, J. Frantti, M. Kakihana, Solid State Ionics 154 (2002) 437.
[11] M.V. Abrashev, A.P. Litvinchuk, M.N. Iliev, R.L. Meng, V.N. Popov, V.G. Ivanov, R.A. Chakalov, C. Thomsen, Phys. Rev. B59 (6) (1999) 4146.
[12] M. Scheithauer, H. Knözinger, M.A. Vanice, J. Catal. 178 (1998) 701.
[13] L.J. Chen, X. Cheng, C.J. Lin, C.M. Huang, Electrochem. Acta 47 (2002) 1475.
[14] J.-M. Giraudon, A. Elhachimi, T.B. Nguyen, F. Wyrwalski, S. Siffert, J.-F. Lamonier, G. Leclercq, XX SICAT, Simposio Ibero-Americano de Catalise, proceeding, in press.
[15] F. Bustamante, F. Cordoba, M. Yates, C. Montes de Correa, Appl. Catal. A: Gen. 234 (2002) 127.
[16] K. Zhou, H. Chen, Q. Tian, Z. Hao, D. Shen, X. Xu, J. Mol. Catal. A: Chem. 189 (2002) 225.

[17] D. Briggs, M.P. Seah, Practical Surface Analysis, second ed., John Wiley, Chichester, 1993.
[18] M. Uenishi, M. Taniguchi, H. Tanaka, M. Kimura, Y. Nishihata, J. Mizuki, T. Kobayashi, Appl. Catal. B: Environ. 57 (2005) 267.
[19] Y. Okamoto, H. Nakano, T. Imanaka, S. Teranishi, Bull. Chem. Soc. Jpn. 48 (1975) 1163.
[20] D.C. Frost, C.A. McDowell, I.S. Woosley, Chem. Phys. Lett. 17 (1972) 320.
[21] J.P. Bonnelle, J. Grimblot, A. D'Huysser, J. Electron Spectrosc. Relat. Phenom. 7 (1975) 151.
[22] G. Sinquin, C. Petit, J.P. Hindermann, A. Kiennemann, Catal. Today 54 (1999) 107.
[23] B. Kucharczyk, W. Tylus, Catal. Today 90 (2004) 121.
[24] L.G. Tejuca, J.L.G. Fierro, J.M.D. Tascon, Adv. Catal. 36 (1989) 237.
[25] S. Petrovic, L. Karanovic, P.K. Stefanov, M. Zdujic, A. Terlecki-Baricevic, Appl. Catal. B: Environ. 58 (2005) 133.
[26] H.P. Bonzel, H.J. Krebs, Surf. Sci. 91 (1980) 489.
[27] C. Moreno-Castilla, M.V. Lopez-Ramon, F. Canasco-Marin, Carbon 38 (2000) 1995.
[28] K. Tabata, I. Matsumoto, S. Kohiki, J. Mater. Sci. 22 (1987) 1882.
[29] B.P. Barbero, J.A. Gamboa, L.E. Cadus, Appl. Catal. 65 (2006) 21.
[30] I. Tan, H. Tanaka, M. Uenishi, K. Kaneko, S. Mitachi, J. Ceram. Soc. Jpn. 113 (2005) 71.
[31] C.F. Cullis, B.M. Willatt, J. Catal. 83 (1983) 267.
[32] Y. Yazawa, H. Yoshida, N. Takagi, S.-I. Komaï, A. Satsuma, T. Hattori, J. Catal. 187 (1999) 15.
[33] A. Ishikawa, S. Komaî, A. Satsuma, T. Hattori, Y. Murakami, Appl. Catal. A 110 (1994) 61.